IEEE Access
Multidisciplinary | Rapid Review | Open Access Journal

Received July 31, 2019, accepted August 15, 2019, date of publication August 20, 2019, date of current version August 31, 2019.

Digital Object Identifier 10.1109/ACCESS.2019.2936538

Electrically-Coupled Goubau-Line-Based Wireless Power Transfer System

BRIAN J. VAUGHN, (Student Member, IEEE), ALDEN FISHER, (Student Member, IEEE), AND DIMITRIOS PEROULIS, (Fellow, IEEE)

Department of Electrical and Computer Engineering, Purdue University, West Lafayette, IN 47907, USA

Corresponding author: Brian J. Vaughn (vaughn22@purdue.edu)

ABSTRACT The first end-to-end Goubau-line-based wireless power transfer system with high efficiency is demonstrated in this paper. The wide spatial distribution of its electromagnetic fields and the lack of significant radiation are two of the most desirable characteristics of the Goubau line for mid-distance wireless powering applications. In this work, we demonstrate a measured RF efficiency of 35% to a single receiver at a distance of 0.5 m for a 233 MHz signal. Further, the performance of multi-receiver power transmission is also examined, as well as the addition of a rectification block, rounding out the wireless power transfer system. Practical advantages of this system over existing state-of-the-art systems are also discussed.

INDEX TERMS Energy harvesting, Goubau line, mid-range, wireless power transfer.

I. INTRODUCTION

Recently, the Goubau transmission line (GLine) wireless power transfer (WPT) system was proposed as a means to improve the range of mid-range wireless power transfer schemes while providing an omnidirectional, asymmetric topology [1]. Efficient solutions to the mid-range wireless power transfer problem have been elusive, with current methods either relying on extreme precision resonant tuning (such as the resonant-coupling WPT technique), or highly lossy techniques (such as far-field WPT) [2], [3]. Furthermore, typically, both the transmitter and receiver must have characteristic sizes that are on the same order of magnitude for the systems to function efficiently. The utility of the GLine structure, however, comes from its flexibility. Using the GLine, power may be efficiently and wirelessly transferred to a near arbitrary number and variety of different receiver structures at once without altering the overall transmitter design, making the scheme valuable for many different applications ranging from wearables to medical implants to Internet of Things (IoT) applications. Further, unlike the mid-range WPT technology pioneered in [2] and [4], the GLine system does not require the transmitter and receiver to be resonators and it is cylindrically symmetric (omnidirectional) [2], [4]. While there currently exist WPT schemes that have a Tx/Rx asymmetry characteristic, are cylindrically symmetric, can transfer power non-radiatively and efficiently ($> 10\%$) at distances exceeding 50 cm, and have been shown to host multiple receivers, no current technology has all of these qualities simultaneously, making the GLine the first of its kind in terms of sheer versatility [2], [5]–[8]. The first ever GLine WPT structure demonstrated in [1] was able to provide power wirelessly to a dipole-like receiver with an 80 MHz RF efficiency of 10% at 0.5 meters away from the transmitter center (this was deduced from the insertion loss of the system; the S_{21} value of the system when connected to 50 Ω reference ports was 10 dB). In this work, we have demonstrated a significant improvement over the GLine WPT first iteration, showing a system that can provide a 233 MHz RF efficiency of up to 35% at 0.5 meters to one receiver, and a combined 233 MHz RF efficiency of 47% to two receivers (where each receiver gets a certain percentage of the input power adding to 47% with both of them located 0.5 meters away from the transmitter center). Additionally, the cylindrical symmetry of the transmitter is investigated, and a five-receiver experiment is conducted to demonstrate the transmitter performance in a potential multi-receiver scenario. Further, this is accomplished using a transmitter with an area that is 37% smaller than that of the first iteration. Finally, tests were conducted with the inclusion of a rectification block on the receiver end, showing the structure's efficacy as a full end-to-end WPT system.

In the proceeding sections, the theory of transmission line wireless power transfer will be discussed, followed by a brief review of GLine field theory and a visualization of the GLine transmitter. Next, a layout of the full design process and

The associate editor coordinating the review of this article and approving it for publication was Lei Zhao.

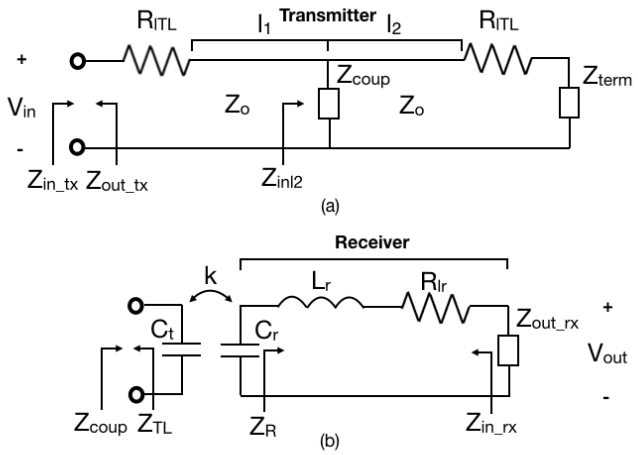

FIGURE 1. (a) Transmission line capacitive WPT equivalent circuit. (b) Section of model that describes receiver coupling.

characterization of the prototype constructed for this work will be discussed.

II. TRANSMISSION LINE WPT THROUGH CAPACITIVE COUPLING

Since transmission lines host both electric and magnetic field propagation, both capacitive and inductive coupling techniques are possible. For the purposes of this paper, only the capacitive case will be discussed, since that is the basis for the prototype system demonstrated in this work. Nevertheless, similar methods as the ones discussed below may be readily applied to the inductive case to derive an analogous formulation.

We begin our analysis with an equivalent circuit model for the transmission line capacitive coupling case, which is illustrated in Fig. 1. Here, Z_{coup} is the impedance seen by the transmission line coupling point when the line is coupled capacitively to an external circuit at some position defined by l_1 and l_2. Z_o is the characteristic impedance of the line (which is modelled as an ideal transmission line), Z_{term} is the impedance used to terminate the line, and R_{lTL} is a loss resistance used to characterize all losses (Ohmic, radiative, dielectric, etc.) along the line. Z_{inl2} is an intermediate impedance used to derive more compact equations. Fig. 1a shows the overall equivalent circuit and Fig. 1b shows the portion of the model that couples to an external receiver circuit for WPT. C_r, L_r, and R_{lr} represent the self-impedance parameters of the receiver structure. C_r, the capacitive part of the receiver, couples to an effective capacitance C_t with a coupling strength defined by a coupling coefficient k. Physically, C_t represents the portion of the transmission line capacitance that interacts with the receiver structure. Clearly, C_t and k are not independent variables, but they may be determined separately as we shall see. For the remainder of the analysis, we will consider a special case of the circuit shown in Fig. 1 defined by the following definitions:

$$l_1 = m_{odd}\frac{\lambda}{4}, \tag{1a}$$

$$l_2 = m_{odd}\frac{\lambda}{4}, \tag{1b}$$

$$Z_{term} = 0 \tag{1c}$$

where m_{odd} and n_{odd} are odd integers. The reasoning behind these choices will be noted in Section IV below, although it is clear that choosing these parameters simplifies the analysis considerably.

With the chosen line lengths and termination in mind, we may use standard circuit theory to deduce the rest of the necessary model parameters as follows:

$$Z_{coup} = [j\omega C_t + \frac{\omega^2 k^2 C_r C_t}{j\omega C_r + Y_R}]^{-1} \tag{2a}$$

$$Y_R = [j\omega L_r + R_{lr} + Z_{\text{out\_rx}}]^{-1} \tag{2b}$$

$$Z_{inl2} = [j\omega C_t + \frac{\omega^2 k^2 C_r C_t}{j\omega C_r + Y_R} + \frac{R_{lTL}}{Z_o^2}]^{-1} \tag{3}$$

$$Z_{\text{in-tx}} = 2R_{lTL} + Z_o^2[j\omega C_t + \frac{\omega^2 k^2 C_r C_t}{j\omega C_r + Y_R}] \tag{4}$$

From this information, we may derive an expression for the power efficiency η from the transmission line input to the receiver output as follows:

$$\eta = \frac{\frac{1}{2}\,\text{Re}(\frac{|V_{\text{out}}|^2}{Z_{\text{out\_rx}}^*})}{\frac{1}{2}\,\text{Re}(\frac{|V_{\text{in}}|^2}{Z_{\text{in\_tx}}^*})} \tag{5}$$

$$\eta = \frac{\text{Re}\left(Y_{\text{out\_rx}}^*\right)}{\text{Re}\left(Y_{\text{in\_tx}}^*\right)}\left|\frac{Z_{\text{out\_rx}} Y_R \omega k \sqrt{(C_r C_t)} Z_o Z_{inl2}}{(Y_R + j\omega C_r)\left(Z_{inl2} R_{lTL} + Z_o^2\right)}\right|^2 \tag{6}$$

This brings us to the determination of C_r, L_r, C_t, and k, all of which may be found using measurement or full-wave analysis simulation. If the receiver is simulated (or measured) alone, C_r may be determined as follows:

$$C_r = \frac{\omega^2 - \omega_o^2}{X\omega\omega_o^2} \tag{7}$$

where X is the receiver reactance at the desired frequency of operation ω, and ω_o is the frequency at which the receiver reactance is equal to 0 (i.e., the resonant frequency of the receiver). L_r is then found using its relation with C_r and ω_o.

If C_r is known and the Z-parameters of the circuit shown in Fig. 1 are also found, C_t and k may be determined. It can be shown that Z_{11} and Z_{21} of the Fig. 1 circuit are expressed as

$$Z_{11} = 2R_{lTL} + j\omega C_t Z_o^2\left(1 - k^2\right) \tag{8}$$

$$Z_{21} = Z_{11}\frac{jkZ_o Z_{inl2}\sqrt{(C_r C_t)}}{Z_{inl2} R_{lTL} + Z_o^2} \tag{9}$$

From here, we may derive C_t and k as follows:

$$C_t = -j\left[\frac{Z_{11} - 2R_{lTL}}{\omega Z_o^2} - j\frac{C_r Z_{21}^2}{Z_o}\right] \tag{10}$$

$$k = \frac{-jZ_{21}C_r}{Z_o\sqrt{(C_r C_t)}} \tag{11}$$

It should be noted that, due to measurement, simulation, or electrical length non-idealities, C_t and k may have non-zero imaginary components in practice. However, as long as $Re(C_t) >> Im(C_t)$ and $Re(k) >> Im(k)$ (greater by at least an order of magnitude), the imaginary components can be safely neglected without compromising the formulation. If this is not the case, or if the derived C_t or k values are non-physical, it is because additional impedance transformations not captured by the model as defined by eqns. 1a-1c are present in the system. Examples of factors that would cause this are the chosen operating frequency or line dimensions not aligning with the model. Because of this possibility, a more generalized empirical design process for transmission line WPT will be discussed in Section IV.

This brings us to our selection of Z_{out_rx} and Z_{out_tx}. The selection of these parameters should be such that η is maximized for a given coupling scenario. If all of the necessary parameters are known, it is straightforward to write an optimization algorithm to determine the optimal output impedances, which will define the matching network circuit design for the system (to be discussed further in Section IV. below).

As a final note, the effective characteristic impedance Z_o may not be readily calculable in all situations. For an unloaded transmission line with a short termination, however, we may write

$$Z_{in} = jZ_o \tan(\theta) \tag{12a}$$

$$\frac{\partial Z_{in}}{\partial \theta} = jZ_o sec^2(\theta) \tag{12b}$$

where θ is the electrical length of the line in radians. If θ is equal to a scalar multiple of π, as is the case in our formulation above, the secant term becomes 1, leading to the following relation:

$$-j\frac{\partial Z_{in}}{\partial \theta} = Z_o \tag{13}$$

Through simulation or measurement, neglecting loss, the derivative term may be determined, allowing us to infer the characteristic impedance of the line.

This concludes the circuit level analysis of the transmission line capacitive coupling circuit defined in Fig. 1 with length and termination parameters defined by eqns 1a-1c. In the next section, we will evaluate the GLine field distribution characteristics to provide context for its efficacy in WPT applications.

III. GOUBAU LINE FIELD THEORY

As demonstrated by Sommerfeld's derivation in [9], solving the homogenous TM_z Helmholtz equation in cylindrical coordinates for a single wire structure of finite diameter and conductivity suspended in free space yields the following cylindrical coordinate field solution:

$$E_r = jE_o\frac{h}{\gamma}Z_1(\gamma r)e^{-jhz}, \tag{14a}$$

$$E_z = E_o Z_0(\gamma r)e^{-jhz}, \tag{14b}$$

$$H_\varphi = jE_o\frac{k_{wav}^2}{\omega\mu\gamma}Z_1(\gamma r)e^{-jhz} \tag{14c}$$

where E_o is the wave amplitude, h is the longitudinal propagation constant, k_{wav} is the wavenumber, ω is the angular frequency, μ is the permeability, γ is a characteristic parameter defined as

$$\gamma^2 = k_{wav}^2 - h^2 \tag{15}$$

and the $Z_i(\gamma r)$ terms are the cylindrical functions that describe the field radially (Bessel functions of the first kind inside the conductor and Hankel functions of the first kind outside it) [9]. This TM mode is the only one that can propagate for this structure and has no cutoff frequency. Fully solving the distribution requires numerical or graphical treatment, as the unknown parameters (h and γ) have only transcendental relationships with the known variables [10]. It should be noted that none of the TM mode fields have a φ-dependence, meaning the structure is cylindrically symmetric.

By inspection, it is not obvious how these fields are more advantageous for WPT applications than, say, the fields of a far-field antenna. However, it can be shown that the normalized derivatives of the transverse E and H-fields are as follows:

$$\frac{\gamma}{jE_o h}\frac{\partial E_r}{\partial r} = \frac{\omega\mu\gamma}{jE_o k_{wav}^2}\frac{\partial H_\varphi}{\partial r} \approx \frac{\partial}{\partial r}\left(\frac{1}{r}\right) \tag{16}$$

Eqn. 16 states that the radial contribution to the rate at which these field magnitudes decrease with distance from the conductor is the same as a 1/r-dependent function, meaning that radially, the GLine fields behave similarly to radiator far-fields. However, the r-component of the real part of the Poynting vector for this mode is many orders of magnitude lower than the z-component, effectively meaning that power is not lost via radial radiation (real power only moves in the longitudinal direction, and this is not radiation, but standard waveguide propagation). To summarize, the transverse field magnitudes of the GLine fall-off radially at the same rate as antenna far-fields, but there is no radiation, meaning that the coupling coefficient to a receiver circuit can remain high for a wide range of distances from the center conductor. This puts the GLine at a distinct advantage over near-field techniques, whose fields also do not radiate, but fall-off as $1/r^2$. Further, radial radiation loss is not a concern for the GLine like it is for standard far-field WPT strategies. These facts make the GLine an attractive candidate for WPT systems. In the next section, the full design process for the GLine WPT system will be laid out in detail as well as visualizations of the GLine fields and characteristics.

IV. GLINE WPT SYSTEM DESIGN AND SIMULATION

The WPT system presented here can be divided into 5 main blocks: the GLine transmitter block, the receiver structure block, the impedance-matching blocks (2 blocks), and the rectification block. Fig. 2 illustrates a block diagram of the full system. Each block is detailed below.

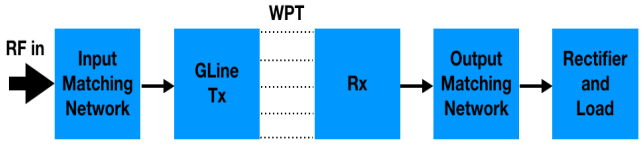

FIGURE 2. GLine WPT system block diagram.

FIGURE 3. Conceptual drawing demonstrating how two GLines could be placed at the two corners of the room. The figure displays the ground planes as wire meshes.

A. GLINE TRANSMITTER STRUCTURE

The GLine transmitter consists of a center conductor and two ''launcher'' structures placed on either end of the conductor wire, with the transmitter input located at the center of one of the launchers and an appropriate termination located at the other. The purpose of the launchers is twofold: they serve to transform the incoming signal at the input from a TEM wave to the GLine TM wave and they contain the field energy of the GLine fields impinging on either end of the center conductor. The most commonly examined launcher topologies are the conical launcher and the planar launcher, along with the quarter-wave balun [1], [11]–[13]. For this work, a circular planar launcher was chosen due to its ease of design and construction, as in [1].

The size of the launchers depends on the desired frequencies of operation. Generally, the lower the frequency, the larger the launcher must be to facilitate efficient power transfer. This is because the energy of the GLine mode extends farther away from the center conductor for lower frequency signals (note the relationship between the unnormalized transverse field derivatives and the frequency) and any field energy that exists outside the launcher radius when the field is incident on the launcher will be lost as scattering and radiation. This means that the smaller the launchers are, the larger the R_{ITL} parameter will be in the circuit model. This also means that any device to be powered by the system must be within the launcher radii to receive power under optimal efficiency conditions. While no theoretical relation exists as of yet for the minimum launcher radius required to achieve a certain RF efficiency, a good rule of thumb for the launcher is to choose a radius that is the larger between the half-wavelength of the lowest desired operation frequency and the maximum desired receiver distance from the center of the transmitter. Each launcher itself may be made up of either a solid conductive disc (which can be implemented as discs of any material covered with copper foil as in [1]) or a wire mesh similar to that which blocks leakage radiation from a microwave oven. Fig. 3 illustrates an example real-world implementation of the GLine transmitter wherein the structure is integrated within the corners of a conference room and the launchers are embedded in or affixed to the floor and ceiling. Such an implementation implies that the launcher size is primarily limited by the size of the room the transmitter is placed in. Note that the design in Fig. 3 uses launchers that are wire meshes. In general, solid discs provide better transmitter performance, but can be more expensive to implement given material need, and the mesh option can provide satisfactory results if designed well. This is discussed further in Appendix I. For the remainder of this paper, though, the disc implementation will be examined exclusively since it is superior in terms of loss.

The termination for the launcher opposite that of the transmitter input should be purely reactive, with open and short terminations being the default choices. The reason for this is that generating a standing wave within the GLine transmitter is currently the best known way of transferring power to a receiver efficiently. Doing so contains the energy to the transmitter space optimally; the only ways energy can leave the system under this condition are through launcher radiation/scattering, input reflection loss, and receiver coupling. If the system termination is resistive, its losses can easily overtake the receiver coupling and reduce the system efficiency. It should be noted that an effect of a standing-wave is the presence of E-field and H-field peaks and nulls along the GLine length. This will be addressed further below.

The length and radius of the center conductor are also important parameters. Solving the TM_z mode reveals that a larger conductor radius generally results in stronger fields within the transmitter, which aids the coupling between the transmitter and receiver. If a short termination is used, then the line length should be an integer number of half-wavelengths around the desired operation frequencies. For instance, a 1 meter line would correspond roughly to 150 MHz, 300 MHz, 450 MHz, etc. Using these exact frequencies is not a stark requirement for the system to function, but using frequencies near the ones above for the 1 meter length case places an E-field null at each launcher plane, considerably reducing launcher loss due to scattering. In the case of an open termination, the line length should be an odd integer multiple of quarter wavelengths of the desired operation frequencies such that the input launcher is located at an E-field null. Although, since the termination launcher is locked at an E-field peak position for this case, it is clear that the short termination is superior from a scattering perspective. This is why eqns. 1a-1c were invoked in the Section I analysis of the transmission line coupling circuit. It should again be emphasized that the GLine WPT system is not a resonant coupling system like the one demonstrated in [2], as any

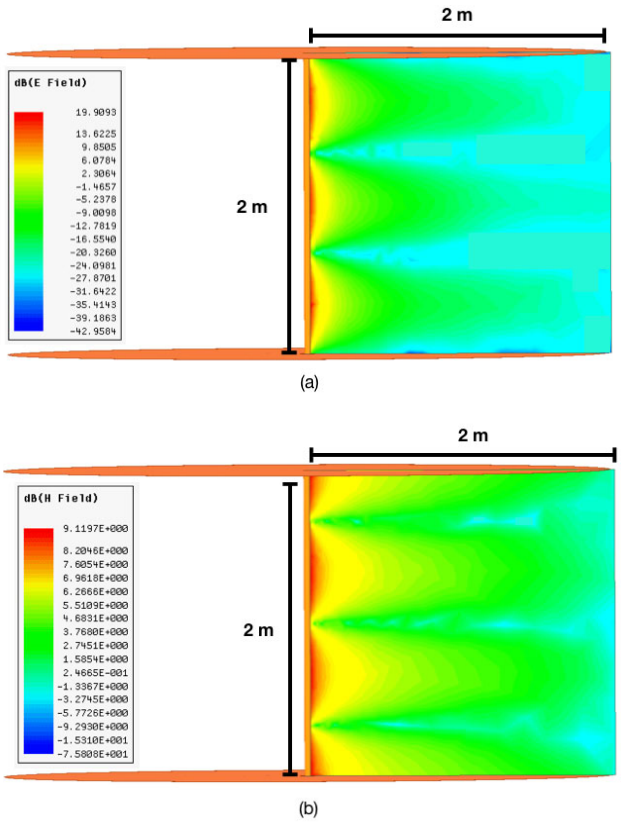

FIGURE 4. (a) Shorted GLine transmitter radial electric field magnitude distribution with 225 MHz, 0dBm incident power. (b) Shorted GLine azimuth magnetic field magnitude distribution with 225 MHz, 1 dBm incident power.

frequency or configuration where the launcher scattering is sufficiently low will do (as opposed to a system that requires tightly-controlled resonant tuning) and the receiver need not be resonantly-tuned, as we will see.

B. GLINE TRANSMITTER SIMULATION

Using ANSYS HFSS, we may simulate the field distribution of the GLine Transmitter. Fig. 4. illustrates the radial E-field and azimuth H-field field magnitude distributions for a 2 meter long shorted GLine excited by a 1 mW excitation. The short is implemented by connecting the center conductor directly to the upper launcher surface. Both launchers have a 2 m radius to maximize the field range. The excitation frequency was chosen to be 225 MHz, the frequency at which the line is six quarter-wavelengths long (or three half-wavelengths). The field plot shows the standing wave nature of the transmitter design with the E and H-field peaks and nulls 90° out of phase.

C. RECEIVER STRUCTURE

Receiver coupling for the GLine system may be either electric or magnetic. For the electric case, an electrically short dipole structure may be used to couple to the GLine radial E-fields, whereas an electrically short loop may be used for magnetic coupling off of the GLine H-fields. Both structure types should be electrically short for two reasons. The first is that electrically-long receivers could get quite large for lower operation frequencies, which is neither desirable nor necessary. The second is that electrically-long receivers can radiate strongly in their own right, so they act as local field scatterers, reducing power transfer efficiency [14]. Note that in [14], it is stated that receiving antenna scattered power cannot necessarily be ''recovered'', so it should not be thought of as available power. Here, however, any power that is scattered by the receiver was present in the GLine system to be used and is now lost, so it was indeed available power. This means that reducing receiver scattering as much as possible is advantageous for coupling efficiency. That said, the receiver should not be too small either, as this will also reduce coupling. In general, having a receiver with a characteristic size between 8% and 25% of the operation wavelength gives reasonable results from a coupling perspective depending on the desired range and efficiency.

As stated in the transmitter discussion, E and H-field peaks and nulls exist along the line due to the standing-wave nature of the distribution. This means that the electric or magnetic coupling strength to the receiver will be dependent on the receiver's longitudinal position along the line, and will too have peaks and nulls if only one type of coupling is used. Receivers that can couple to both electric and magnetic fields (or transmitters that can move its field peaks around) are beyond the scope of this work, but more complex receivers than the types presented here are possible.

D. IMPEDANCE-MATCHING

The GLine WPT system presented here requires input and output impedance matching networks which will tune Z_{out_rx} and Z_{out_tx} to their necessary values to maximize transfer efficiency. In this work, these matching networks are static LC topologies. Three methods may be used to design the matching circuits assuming 50 Ω systems, each depending on the anticipated coupling strength and design methodology. The first is the method discussed in Section II based on the equivalent circuit model for the system. The second, which is more general, is to place the receiver at the position within the GLine transmitter where optimum coupling is desired, extract the 2-port Z-parameters for the desired operation frequency, use the relationship between Z and S-parameters (which may be found in [15]) to numerically optimize the system output impedance values (Z_{out_tx} and Z_{out_rx}), and design networks that match 50 Ω ports to these optimal impedances. The third, which is more straightforward but sub-optimal for stronger coupling scenarios, is to match the receiver antenna to 50 Ω without any transmitter coupling, place the receiver (with its matching network loaded with a 50 Ω termination) at the desired optimum coupling position, and match the resultant transmitter input impedance at the desired frequency of operation to 50 Ω. Often, these three methods yield similar matching networks, but the third method is more suited for a modular implementation.

It should be noted that the Q factors of the components in the matching circuits can affect the overall system efficiency non-negligibly. Generally, the shorter the receiver is electrically, the more extreme the component values must be if the coupling is low, increasing losses. This presents another trade-off between the receiver size and the maximum possible efficiency that can be achieved with available components.

Finally, it should be noted that with static networks, the system can only be optimally matched to one receiver position at a time. This is not to say that the efficiency at all other positions will be unacceptably low, as will be seen in Section VI., but it does mean that the efficiency at positions other than the design position will be lower than they would be if the matching networks were designed around said positions.

E. RECTIFICATION BLOCK

The rectification stage used for this work has the same topology as that demonstrated in [16], consisting of a low-pass filter (to suppress reflected harmonics from the diode) and a single shunt-configured diode with lumped-element impedance matching components. It is terminated with a 2.7 kΩ load. Note the rectifier that will be used in the following section has static matching and is optimized for 233 MHz while the one in [16] has variable matching and is optimized for 82 MHz with a different load. Regardless, the operation of both circuits is functionally the same. See [16] for more details on the rectifier operation and design topology.

F. A NOTE ON GLINE SIMULATION

Simulating both the transmitter and receiver of the GLine WPT system gives the designer insight on the losses of both while also giving valuable information about the coupling potential between the two structures, making simulation a valuable design step. However, simulating the system with the accuracy necessary to design adequately precise impedance matching networks is quite difficult. This is because the transmitter and receiver vary greatly in size, so generating sufficiently refined simulation spaces is challenging from a computer memory perspective when they are simulated together. Further, the responses of both the transmitter and receiver are affected by their surrounding environment, which cannot be feasibly simulated in most cases. The effect of this is that the simulation will generally imply that R_{ITL} is significantly smaller than it actually is at certain frequencies. This means that, while simulation is certainly necessary for establishing foundational characteristics of the transmitter, the receiver, and the interaction between them, any Z-parameters and matching networks generated from simulation alone will most likely not result in the expected efficiency output. This means the optimal efficiency predicted by simulation may not be truly reflective of what is possible even under ideal laboratory conditions, and thus, GLine simulation can only give a rough estimation of the system performance.

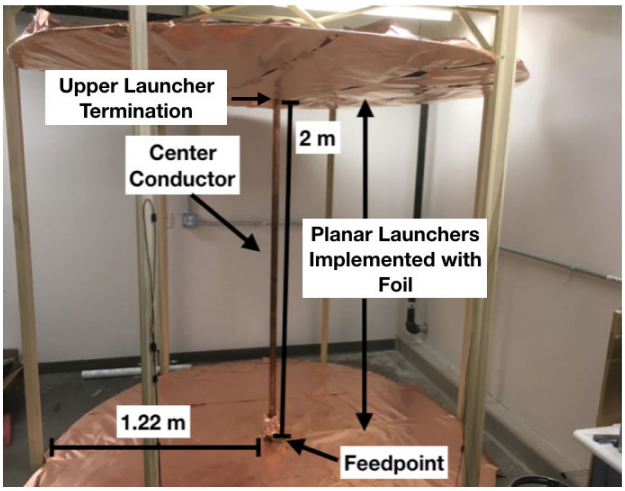

FIGURE 5. Constructed GLine transmitter proof-of-concept prototype.

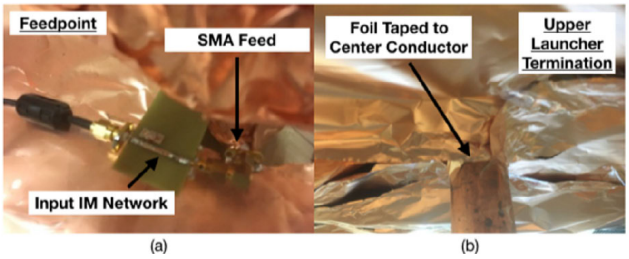

FIGURE 6. Zoomed-in images of (a) constructed GLine transmitter feed and (b) short-circuit upper launcher termination.

V. CONSTRUCTED GLINE SYSTEM RESULTS

A GLine transmitter, an electrically-coupled receiver set, a matching circuit set, and a rectifier were constructed at Purdue University for experimentation. The transmitter center conductor is approximately 2 m long and 4 cm in diameter. The launcher radii are 1.22 m and each launcher was built by affixing copper foil to plywood discs connected to a wooden frame. A short termination was implemented by taping copper foil between the center conductor and the upper launcher (the foil is conductive on both sides). The feed, placed at the center of the lower launcher, was constructed by soldering the center conductor of an SMA connector to a strip of copper foil, soldering the grounding plate of the connector to another strip of foil, and taping the strips to their appropriate contact points (strip 1 to the GLine center conductor and strip 2 to the lower launcher surface). Additionally, a cluster of copper foil was wrapped around the center conductor near the feed interface. This reduces leakage radiation at the feed, decreasing losses. The transmitter is pictured in Fig. 5 and Fig. 6.

It was found that R_{ITL} was smallest at 233 MHz for this construction. At this frequency, the standing wave E-field magnitude is small at the launchers, minimizing scattering loss. Further, this frequency keeps the receiver size reasonable without requiring extreme impedance matching networks. For these reasons, data at frequency points centered

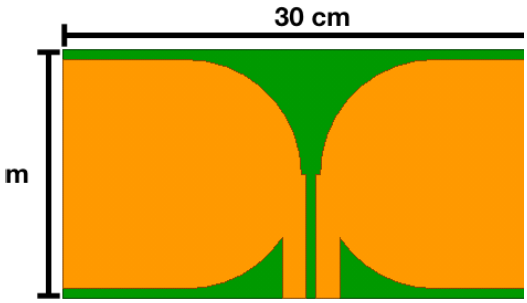

FIGURE 7. Planar dipole receiver structure.

around 233 MHz will be discussed. Note that the frequency of operation is not 225 MHz (the frequency at which 2 m is 1.5 wavelengths) due to the nature of the launcher connections and surrounding environment altering the apparent electrical length and scattering profile of the line. Also note, again, that while the frequency where the E-field is minimized at both the launchers may be a resonant frequency of the line, the coupling of the system is not resonant in nature, and any frequency around said resonant frequency where the scattering loss is low enough may be used. In any case, the unloaded reactance of the transmitter for this work was not zero at 233 MHz, so this operating frequency is not truly a resonant one.

The receiver used in the measurements is a planar dipole whose structure and dimensions are pictured in Fig. 7. It is made on a 1 mm thick FR-4 substrate and is designed to couple off of the E-field of the GLine standing wave.

The impedance matching circuits are designed such that, when the receiver is placed approximately halfway up the line and its center is 0.5 m away from the center conductor, the coupling between it and the transmitter is optimal for a 233 MHz signal. To this end, the GLine feed matching network was designed to match a 50 Ω port to 6.4–26.4j Ω and the receiver matching network was designed to match a 50 Ω port to 18.5+17j Ω.

To clarify, this means that the impedance that the GLine feed sees when looking through its matching circuit to a 50 Ω port is 6.4–26.4j Ω, and the impedance the receiver sees when looking through its network to a 50 Ω port is 18.5+17j Ω. These impedances are Z_{out_rx} and Z_{out_tx} of the system. The matching circuits were designed by applying method 2 from the matching network construction explanation in the Section IV. of this paper after the Z-parameters were measured. They were implemented as LC matching circuits using Kemet chip capacitors and Coilcraft air-core inductors, although any sufficiently high Q components and techniques may be used.

The rectifier was built using standard lumped elements and an SMS3922 Schottky diode. It is designed to rectify incident signals at powers ranging between −10 and 20 dBm, but can be re-optimized to accept higher or lower powers [16].

To characterize the GLine WPT system, multiple coupling scenarios were evaluated. First, the RF efficiency (i.e., the insertion loss of the system from the GLine feed matching

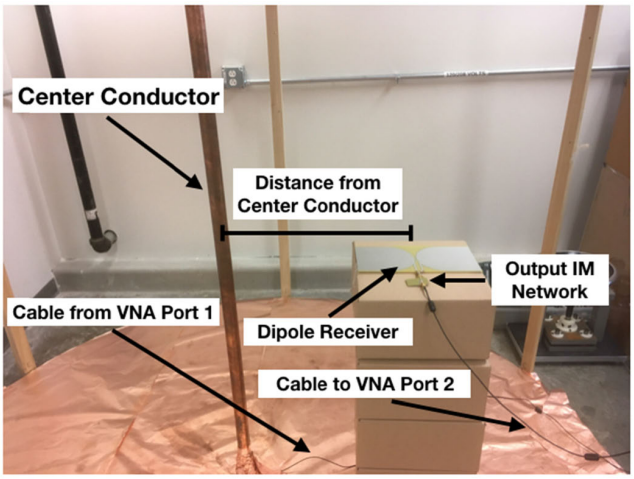

FIGURE 8. One-receiver test setup.

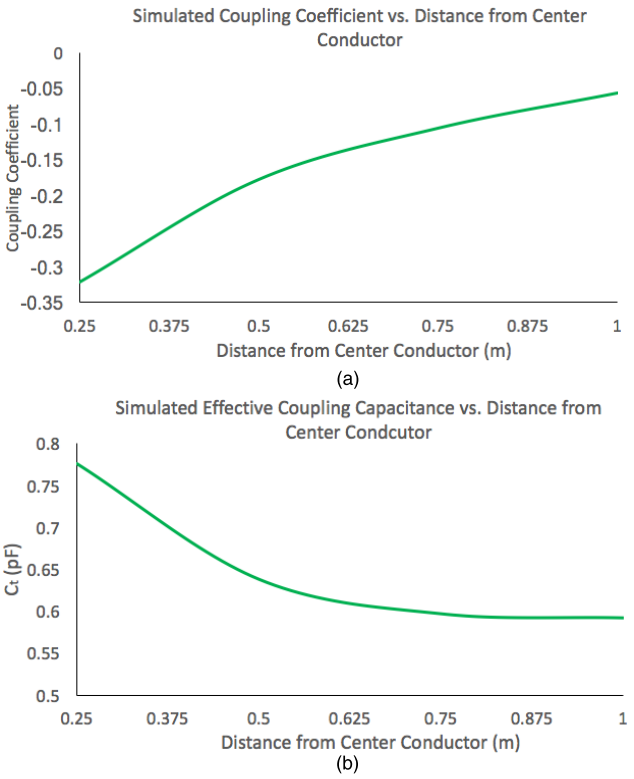

FIGURE 9. (a) Simulated coupling coefficient k as a function of receiver distance from the center conductor at 233 MHz. (b) Simulated coupling capacitance value as a function of receiver distance from the center conductor at 233 MHz.

network input to the receiver matching network output) was measured and compared to simulated values. The measurement was conducted by using a vector network analyzer (VNA) to extract the S_{21} values of the system when the receiver was placed on a cardboard stand approximately 1 m above the lower launcher surface (about half-way up where an E-field peak exists) and at variable distances from the center conductor. The impedance matching networks were kept static for these measurements. Note that for accurate measurement, the VNA was placed outside of the transmitter

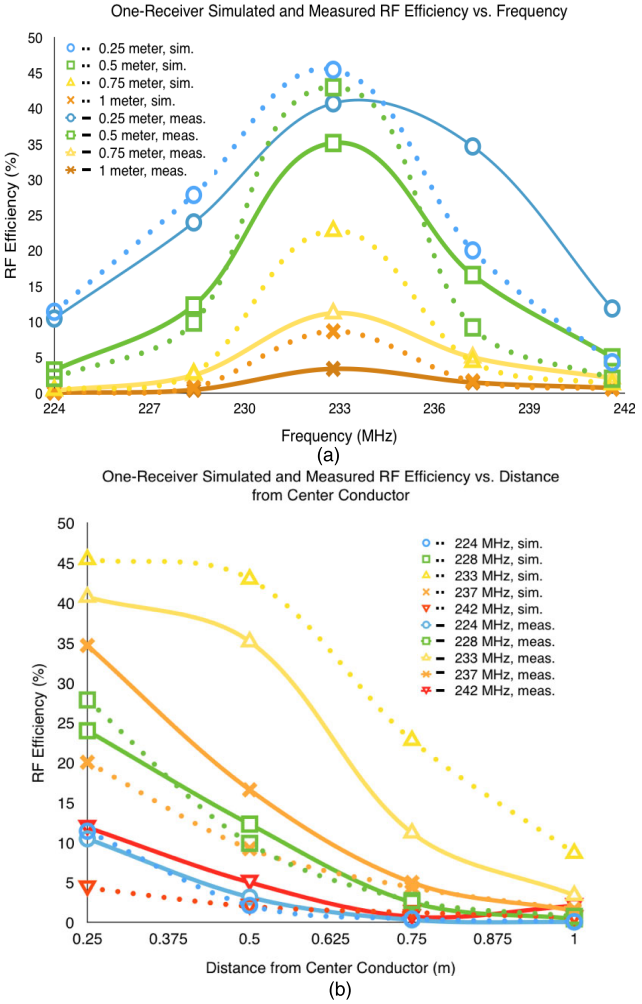

FIGURE 10. One-receiver simulated and measured RF efficiency as a function of (a) frequency and (b) distance.

and the measurement cables had RF chokes affixed to them (ferrite beads were used), otherwise the GLine fields would couple to the VNA ground plane and cables, throwing off the calibration. Note also that standing inside the transmitter affects the results (since the human body changes the impedance profile of the system), although not by very much unless person is very close to the receiver position or the center conductor. For the purposes of this work, the transmitter space was kept empty save for the receivers and their stands.

The receiver dipole is oriented such that the radial GLine fields run along the dipole length so it is co-polarized with the coupling E-field. This is required; if the dipole is not aligned with the radial field, coupling decreases dramatically. Fig. 8 illustrates the measurement setup. Fig. 9 and Fig. 10 show the simulated coupling coefficient and C_t values, and the RF efficiency data (both measured and simulated using ANSYS HFSS and ADS at 233 MHz) respectively. The line characteristic impedance was found to be 187 Ω from simulation. Note that the effect of the measurement cables has been calibrated out of the measurements. Also, the length of the line in the simulation was reduced from 2 m to 1.95 m. This is to account for an apparent electrical length difference

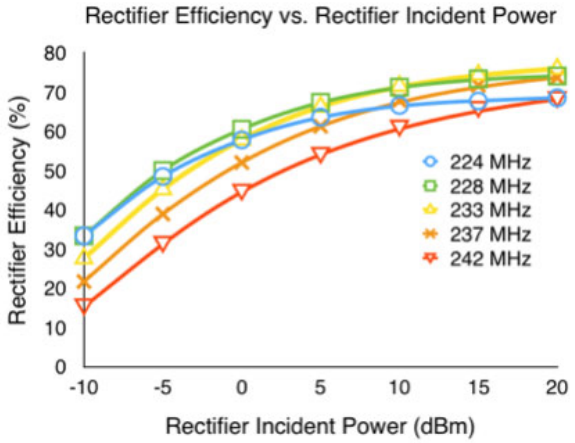

FIGURE 11. Rectifier measured efficiency data.

between the construction and simulation model caused by the termination foil contact point being lower than the center conductor tip.

Next, the total efficiency of the system (i.e., the efficiency of the system from the input of the GLine matching circuit to the output on the rectifier load) was measured. This was done by connecting the system input to a signal generator and power amplifier, connecting the receiver output to the rectifier, and sweeping the signal frequency, receiver position, and transmitter input power, measuring the efficiency at each data point. The incident power of the rectifier was also measured by placing using an intermediate RF coupler and power meter. Again, all losses not associated with the WPT system were calibrated out. Fig. 11 outlines the efficiency of the rectifier alone as a function of rectifier incident power and Fig. 12 illustrates the total efficiency data of the system as a function of rectifier incident power.

Next, another planar dipole receiver was constructed and measured simultaneously with the first at the same height. The receivers are identical in structural design, but the second was made with a 1.27 mm thick Rogers 5880LZ substrate. It's output impedance was matched to 9.8+25.7j Ω (determined using the same method as with the first receiver). With this second antenna, two-receiver power transfer as well as the cylindrical symmetry of the transmitter were examined. The RF efficiency was extracted at one receiver while the other was terminated with a 50 Ω load for all measurements. Note that the GLine and first receiver matching networks were not altered.

During each measurement, both receivers were placed approximately 1 m up the line at the same distance from the center conductor, but they were offset by an azimuth angle θ with respect to the center conductor, with one receiver at a stationary position while the other was rotated around the transmitter center. θ was swept between 45 and 315 degrees at several receiver distances. Fig. 13 illustrates this setup. Fig. 14 details the RF efficiency and power split ratio performance (i.e. the percentage of the total received power each receiver consumes both adding to 100%) with respect to θ

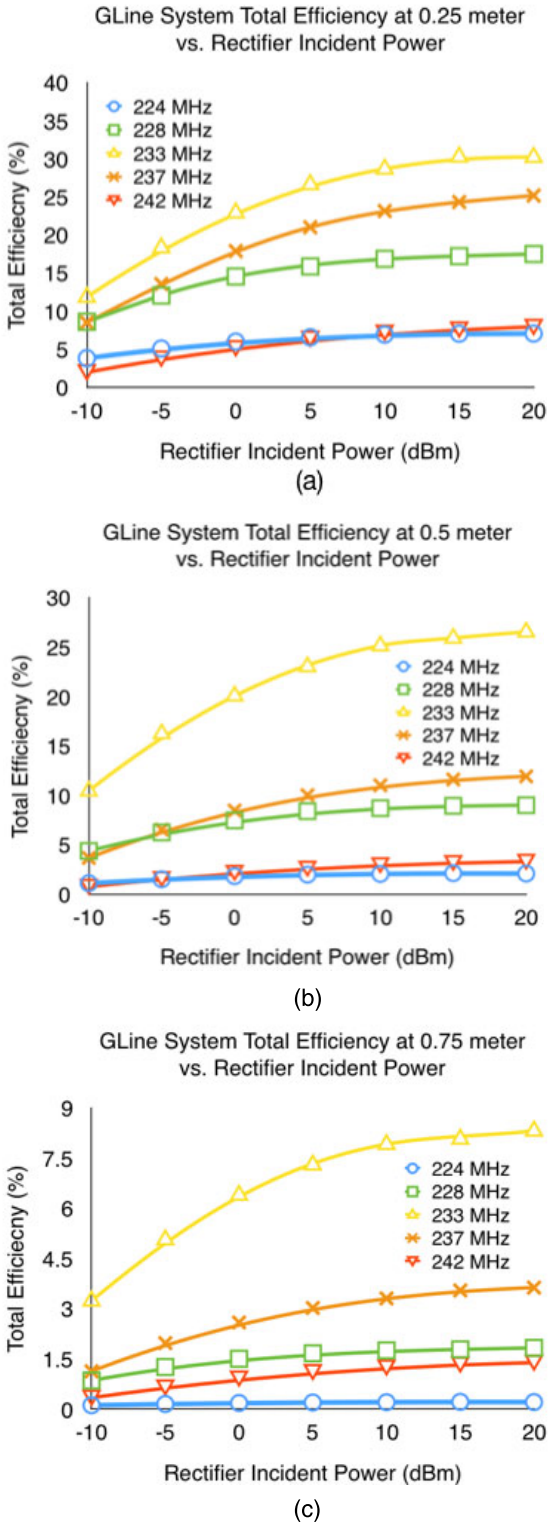

FIGURE 12. One-receiver GLine system measured total efficiency for 0.25 m (a), 0.5 m (b), and 0.75 m (c) distances.

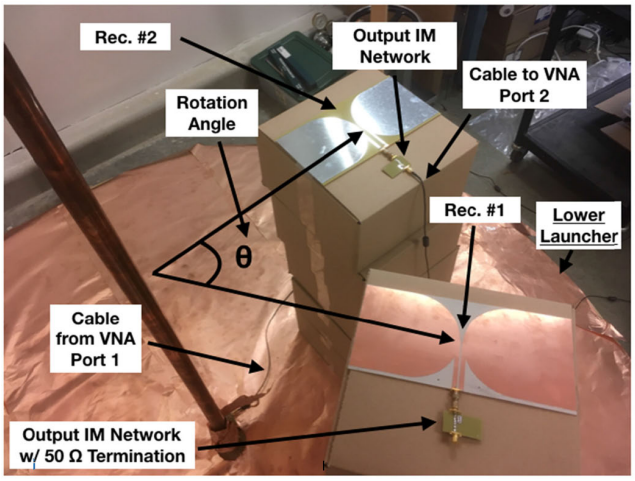

FIGURE 13. Two-receiver measurement setup.

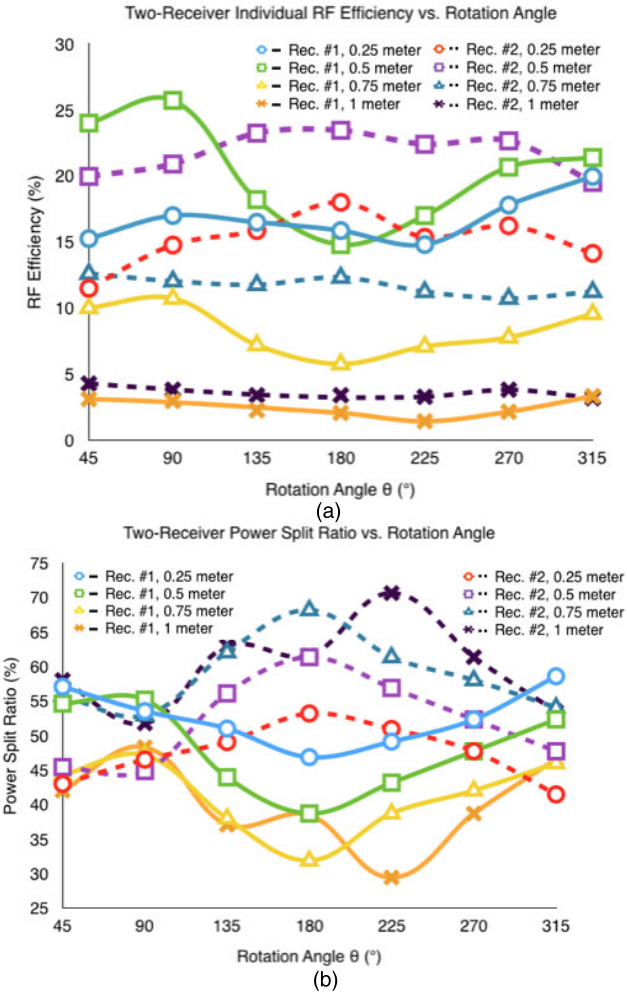

FIGURE 14. (a) Two-receiver RF efficiency and (b) power split ratio with respect to rotation angle at 233 MHz.

at 233 MHz for different receiver distances. Fig. 15 shows the individual RF efficiency with respect to frequency when θ is 90 degrees. Here, receiver #1 is the 5880LZ dipole (the rotating receiver) and receiver #2 is the FR-4 dipole.

Finally, an experiment was conducted where five receivers, including the ones described above, were placed at various positions surrounding the center conductor, all at a 1 m height.

The additional antennas were all planar dipoles of various sizes constructed with copper tape on FR-4 substrates of

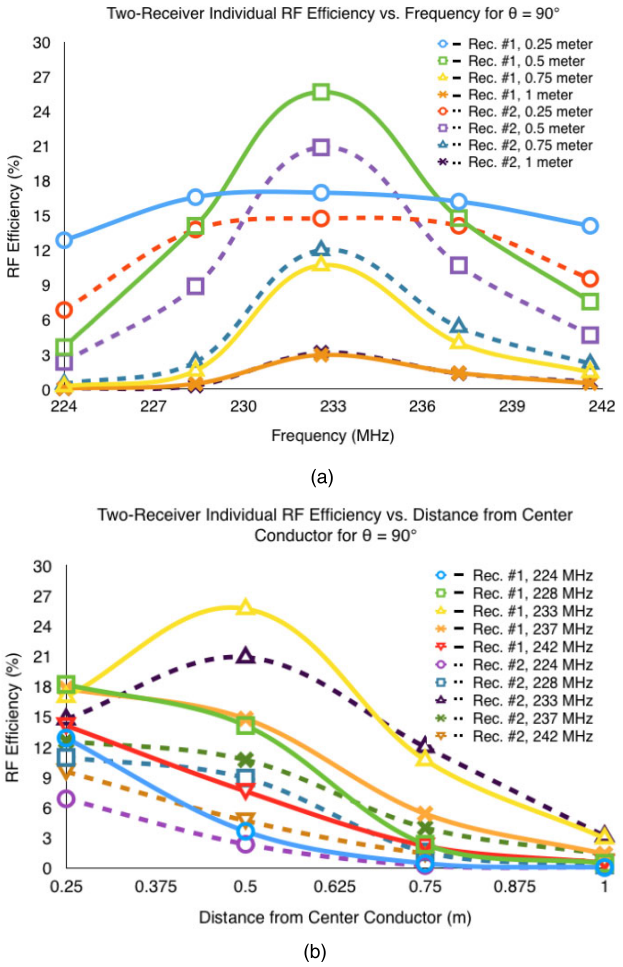

FIGURE 15. Two-receiver RF efficiency with respect to (a) frequency and (b) distance for $\theta = 90°$.

differing thicknesses between 0.4 mm and 1.6 mm. Each receiver was placed 1 m up the line at various distance and θ locations and they were matched to 50 Ω while in position with at least a 10 dB return loss. The return loss of each receiver was measured while every other one and the transmitter input were terminated with 50 Ω loads. In this way, a potential real-world multi-receiver scenario was demonstrated. To extract each receiver's RF efficiency, the output of one receiver at a time was connected to a VNA while all others were terminated with 50 Ω loads, same as the two-receiver test. Note that placing five receivers in the transmitter loaded the GLine significantly such that its input impedance was 24–43j Ω, so the transmitter matching network was switched out to better match to the loaded impedance at 233 MHz. Fig. 16 illustrates the multi-receiver experiment setup and Table 1 details the size, position, and RF efficiency of each receiver.

VI. RESULTS AND DISCUSSION

Referencing Fig. 10, it can be seen that the maximum measured RF efficiency for the one-receiver case is 40% at 0.25 m, 35% at 0.5 m, 11% at 0.75 m, and 3% at 1 m when

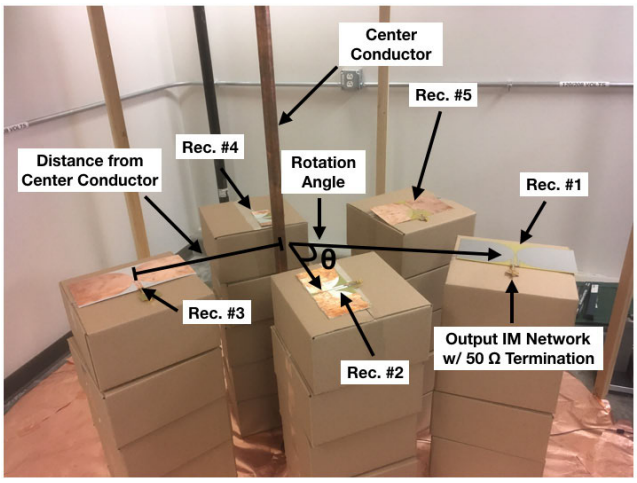

FIGURE 16. Multi-receiver test setup.

the matching circuits are optimized for the 0.5 m distance and 233 MHz. It should be noted that efficiency obtained with this implementation is substantially higher than that observed in [1]. The reasons for this stem from the launcher construction, the receiver design, and the impedance matching network components. The launchers in [1] were made from cardboard sheets and as such were susceptible to bending, disrupting the field containment. The dipole used in [1] was a prototype made from soldering wires in a bowtie-like configuration, but the solder joints created lossy conduction sites that lowered transfer efficiency. Finally, the capacitors and inductors used here have much improved Q-factors compared to those in [1]. All of these factors led to a large efficiency improvement.

Fig. 10 also shows that the difference between the simulation and measurement is quite pronounced for larger distances. This can be explained by the note on GLine simulation in Section IV. of this paper. The simulation had the GLine transmitter suspended in a vacuum, while the implemented system was surrounded by walls and equipment. The closer the receiver is to these interferers, the more they affect the receiver's self-impedance, creating an impedance mismatch factor that was not present in the simulation.

This is also why the measured and simulated results are closer when the receiver distance is smaller. Other deviations can be explained by losses caused by feed radiation, launcher scattering, surrounding object interference, simulation inaccuracies, and a slightly uneven launcher surface (the foil taped to the upper launcher sags differently in different spots, causing some field reflection asymmetry).

An interesting detail of Fig. 10 is that the measured efficiency bandwidth for every receiver position is higher than the simulated case. This also can be attributed to factors in the built system that were not captured by simulation. This effect is most likely a product of the matching circuit aberrations (parasitics, electrical lengths, etc.). It should be noted that the simulated feed and receiver output impedances were 13-28j Ω

TABLE 1. Multi-receiver experiment data.

Receiver #	Size (cm²)	Distance (m)	θ	RF Efficiency (%)	Total Combined RF Efficiency (%)
1	450	0.66	0	4.7	-
2	260	0.36	45	11.75	-
3	450	0.44	135	13.5	-
4	90	0.2	225	2.4	-
5	320	0.47	315	5.9	-
All	-	-	-	-	38.25

and 19+20j Ω respectively, and that the cardboard receiver stand was not included in the simulation.

From Fig. 12, we see that the total efficiency is maximized when the rectifier incident power is 20 dBm. This is a consequence of the rectifier diode non-linearity [16]. The maximum total efficiency of the system was 30% for 0.25 m, 26.5% for 0.5 m, and 8.3% for 0.75 m. 1 m measurements were not taken due to the high input power required to observe the relevant rectifier incident power at each frequency. These results correspond to an optimal rectifier efficiency of 75% at 233 MHz, which is consistent with measurements taken of the rectifier alone.

As seen from Fig. 14 and Fig. 15, when $\theta = 90°$, the maximum RF efficiencies for receiver #1 are 17% at 0.25 m, 26% at 0.5 m, 11% at 0.75 m, and 3% at 1 m. The maximum RF efficiencies for receiver #2 are 15% at 0.25 m, 21% at 0.5 m, 12% at 0.75 m, and 3% at 1 m. The maximum combined RF efficiencies are therefore 32% at 0.25 m, 47% at 0.5 m, 23% at 0.75 m, and 6% at 1 m. For this scenario, the power split between the receivers is approximately 55/45. However, there is substantial deviation from the theoretical 50/50 power split when θ is between 135° and 225° for distances above 0.25 m. This can be attributed to the fact that the transmitter is adjacent to a wall and electrically large piping, leading to field distortion and receiver impedance detuning on the side closest to those elements. This is supported by the high cylindrical symmetry when both receivers are close to the transmitter center (and thus more isolated from environmental field distortion effects), as well as when both receivers are on the same half of the transmitter (when θ is either greater than 90° or less than 270°). Even so, the highest deviation constituted a 30/70 power split and no azimuth nulls were present. Another notable detail is that, unlike in the single-receiver case, the RF efficiency was higher at a 0.5 m distance than a 0.25 m distance. This is because when the receivers are both placed near the transmitter center, there is significant cross-coupling between the two, which causes impedance mismatch since the matching circuits were designed independently. The transmitter input is also detuned under this condition since the effective coupling of the system is substantially higher. While a full two-receiver theoretical analysis is not presented here, adding an identical receiver effectively halves Z_{coup} and doubles the coupling contribution to the RHS of eqn. 4 in the Section II formulation, which explains the impedance drift. This can be fixed if the optimal receiver position is set to 0.25 m and the matching circuits are designed simultaneously, but that is beyond the scope of this work. Finally, it is apparent that the individual RF efficiency values of the two receivers are less than the RF efficiency of the one-receiver case. This is due to the introduction of another loss element in the system when another receiver is added. Referencing the formulation of Section II, adding another receiver introduces another R_{lr}

TABLE 2. WPT technology feature comparison.

Scheme	Mid-Range[1]	Multiple Receivers	Cylindrical Symmetry	Requires Resonance	Astmmetry Factor	Mid-Range RF Efficiency (d = 0.5 m) [3]	Receiver Cross-Sectional Area (m^2)	Receiver Volume (m^3)
This Work	Yes	Yes	Yes	No	6.67	35%	4.5E-02	4.5E-05
[2]	Yes	No	No	Yes	1	95%	2.827E-01	5.655E-02
[5]	No	Yes	Yes	Yes	3.33	-	2.83E-03	1.424E-06
[6]	Yes	No[2]	Yes	Yes	1	10%*	5.03E-03	5.78E-04
[7]	Yes	No	No	Yes	2	26%*	1E-02	4E-06
[8]	Yes	No	Yes	Yes	1	-	4.0E-02	2E-02

[1] Technique is considered mid-range here if the RF efficiency at d = 0.5 m is 10% or more.
[2] Feature may be possible, but is undemonstrated in cited work.
[3] Asterisks indicate efficiency was linearly extrapolated from data given in cited work. If cell has no entry, there was not sufficient information from cited work to determine efficiency.

component (see Fig. 1b). The new R_{lr} and the increased effective coupling coefficient k have competing effects, so even though the combined efficiency of the two-receiver case can exceed the efficiency for one receiver, the RF efficiencies of each individual receiver will not reach that of the one-receiver case for the same distance unless the receiver antennas are completely lossless.

Table 1 details the results for the five-receiver experiment. As can be seen, the individual efficiency of each receiver varies from 2.4% to 13.5%, with the RF efficiency of all the receivers combined totaling at approximately 38%. The variability of the efficiencies can be attributed to the size of each receiver, as well as their positions with respect to the transmitter and the environment outside the transmitter. For instance, receiver #1 (see Fig. 16), while among the largest of the receivers, was placed significantly farther away from the center conductor than the others, so it received less power than smaller receivers. This demonstrates that other coupling factors, particularly position, matter more than receiver size alone. It should also be noted that splitting the power between five receivers lowered the max individual RF efficiency each receiver could achieve while the others are also receiving power. Nevertheless, a combined RF efficiency of 38% was realized, exceeding the one-receiver case.

VII. CONCLUSION

The design process of the GLine WPT system has been laid out and a working electrically-coupled WPT structure has been demonstrated. At a 0.5 m distance from the center conductor for a 233 MHz signal, the achieved one-receiver RF and total efficiencies were 35% and 26.5% respectively, a two-receiver combined RF efficiency of 47% was observed for the same distance, and a five-receiver combined RF efficiency of 38% was obtained. Table 2 shows a feature and metric comparison between the GLine scheme and other recent/foundational WPT topologies, highlighting the GLine topology's merit. Three factors to note about this table:

1.) Only the receiver dimensions were highlighted in Table 2 because this is the most prohibitive profile metric. If the transmitter provides positional freedom for the receiver, the former may be placed in a non-disruptive location, such as a wall, the floor, or a ceiling. In the GLine's case, the launchers, while large, can be embedded in the floor and ceiling in such a way that does not sacrifice space. The wooden frame of the prototype above would also be omitted from such a practical implementation. The center conductor, meanwhile, can be placed in the corner of a room or any spot where a pole-like structure is acceptable, so it is no more disruptive than a tall, thin piece of furniture. However, for many

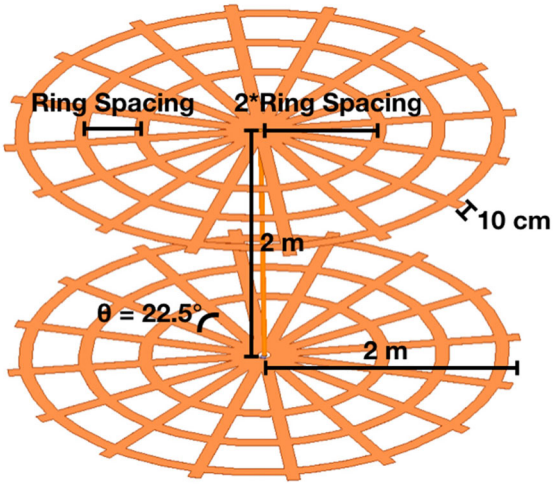

FIGURE 17. GLine transmitter with mesh launchers; three rings shown.

applications such as portable electronics, wearables, sensors, implants, IoT etc., a smaller receiver profile is preferable, so its dimensions were listed.

2.) Not all of the works listed in Table 2 gave efficiency data for a 0.5 m separation distance. As noted in the footnote, the efficiency data for [6] and [7] was extrapolated linearly from the data that was given in these papers. This is a valid approximation based on the efficiency fall-off rate for the measurements taken in [2] and the fact that the techniques of [6] and [7] are resonant. No efficiency metrics were given in [5], so its entry was omitted. In [8], an RF efficiency of 0.35% was given for a 7 m distance and no data was taken for a distance less than 2 m, which was not enough information to infer an efficiency metric for 0.5 m. It is assumed, however, that the 0.5 m RF efficiency for that work exceeds the 10% threshold to be considered a "mid-range" technique as defined in this work.

3.) The asymmetry factor of the system is computed by dividing the largest dimension of the transmitter or receiver (whichever is larger) by the largest dimension of the other element. For the GLine, the largest dimension was 2 m instead of 2.44 m since, again, embedding the launchers in the floor and ceiling makes their diameters less relevant.

The data presented in this work establishes the state-of-the-art for the GLine WPT system, the only current non-radiative, mid-range scheme that simultaneously is asymmetric, is omnidirectional, can host multiple receivers, and does not require resonant coupling.

APPENDIX I
MESH LAUNCHER ANALYSIS

In order to examine the efficacy of the wire-mesh launchers shown in Fig. 3, a simulation case-study was conducted in HFSS to determine the loss characteristics of planar mesh launchers. Fig. 17 shows the design of such a structure with a shorted termination. Here, the launchers are formed by a series of concentric rings connected by a star formation

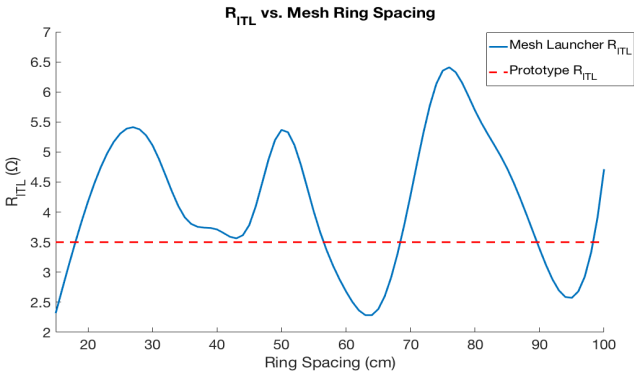

FIGURE 18. Mesh launcher transmitter R_{ITL} as a function of ring spacing for 225 MHz excitation.

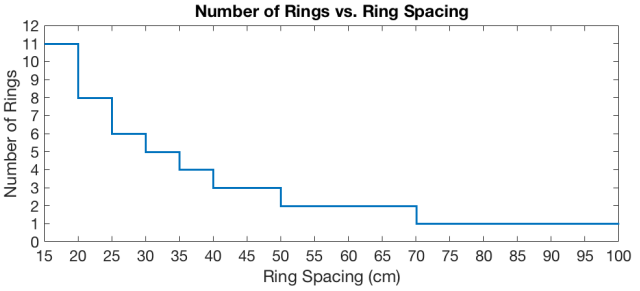

FIGURE 19. Number of rings in mesh launcher as a function of ring spacing.

TABLE 3. HFSS human phantom dielectric parameters.

Phantom Section	ε_r	σ (S/m)
Head	48	0.83
Body	59.75	0.867

of conductive strips. In the study, the spacing between the rings was swept between 15 and 100 cm. If the radius of a ring exceeded 2 m, the ring was omitted from the launcher. The inner-most ring had a radius that was twice the ring spacing, meaning that fewer and fewer rings were included as the ring spacing increased. For each configuration, R_{ITL} at 225 MHz was extracted. In Fig. 18, the simulated R_{ITL} for each ring spacing is plotted compared to the R_{ITL} value of the constructed prototype, which was approximately 3.5 Ω. Fig. 19 shows the number of rings included for each ring spacing.

It is evident from Fig. 18 that R_{ITL} is a somewhat periodic function of ring spacing. This is because the apertures created by the space between conductive surfaces lead to interference patterns that either facilitate or cancel field leakage. Because of this, there are distinct regions where R_{ITL} is minimized. Two such regions are around when the ring spacing is 65 cm with two rings and when the ring spacing is 95cm with only one ring. In both of these regions, the simulated R_{ITL} is lower than the measured value of the prototype shown previously, indicating mesh launcher feasibility. A more in-depth

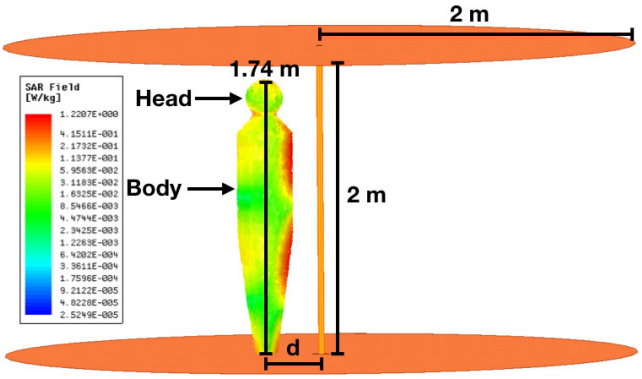

FIGURE 20. Human phantom positioned inside GLine transmitter for SAR simulation.

analysis is beyond the scope of this work, but this study shows that mesh launchers serve as a tenable solution for GLine launcher design.

APPENDIX II
SAR SIMULATION

Since many potential GLine applications involve humans standing within the transmitter area, the question of electromagnetic safety arises. To address this on a base level, simulations were conducted in HFSS at 225 MHz to determine the Specific Absorption Rate (SAR) characteristics of the system. A homogeneous human phantom made up of a head and body was constructed in HFSS using parameters derived from the contents of IEEE Std 1528-2013 [17]. The parameters are given in the table below.

Note that the table at the end of [17] does not list values at 225 MHz exactly. As such, the values above were extrapolated from the given data.

To characterize the SAR, the human phantom, pictured in Fig. 20, was placed at set distances from the center conductor of a GLine transmitter while the input power was swept between −30 and 10 dB (1 mW−10 W). The height of the phantom is 1.74 m, the radius of the head is 12 cm, and the radius of the body's trunk region is 18 cm. The distance from the center conductor is defined from the center axis of the phantom. The local SAR was simulated for each case and the peak values in both the head and body are plotted in Fig. 21 against the 1.6 W/kg limit mandated by the FCC. Note that the local SAR provides a more conservative metric for this study since it will always be larger than the SAR averaged over a region greater than a single mesh cell.

Fig. 21 shows that the peak local SAR is well below the FCC limit for most of the cases simulated. The threshold is crossed when the phantom center is positioned 0.25 m away from the center conductor and the input power is approximately 3.25 W. Many applications, however (e.g., implants, wearables, sensors, etc.), can be accommodated with input powers far less than this. Note that the head SAR was markedly less than the body SAR for all cases. This is because of the head's position in the standing wave distribution as well

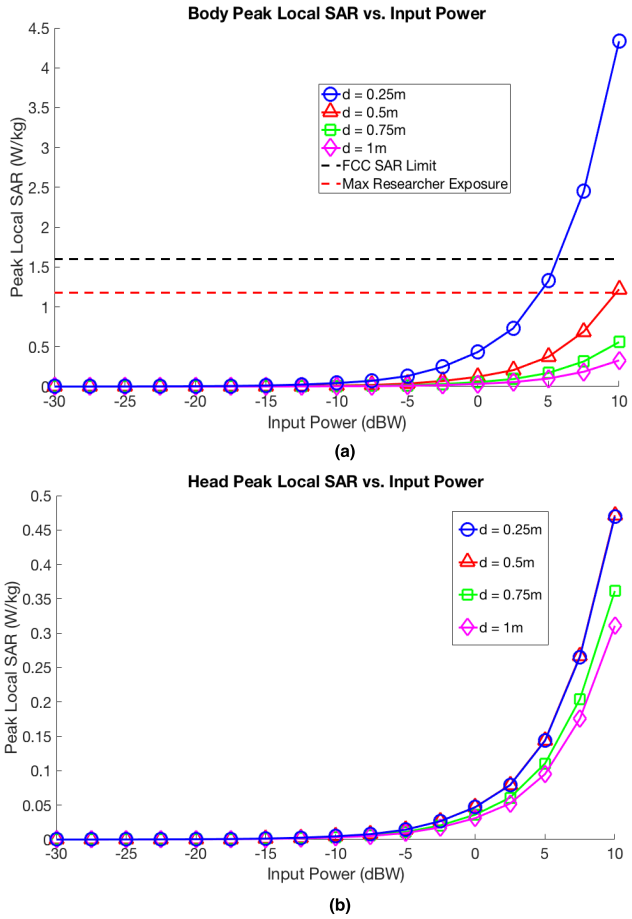

FIGURE 21. (a) Simulated peak local SAR in phantom body as a function of input power and (b) simulated peak local SAR in phantom head as a function of input power. The researchers' maximum exposure during experiments is also shown.

as the fact that its outer surface was always 6 cm father away from the center conductor than the body's outer surface due to the difference in radius. Given the comparison between the head and body homogenous dielectric parameters, it is concluded that the body SAR values can be treated as a valid worst-case scenario nevertheless.

APPENDIX III
FCC FREQUENCY ALLOCATION

The prototype constructed in this work operates at 233 MHz, which is within a restricted band in the United States. However, there is an amateur radio band close-by that includes frequency allocation from 222 MHz to 225 MHz [18]. Operation inside this band is easily within the capabilities of the GLine, so it could be designed for that range, nullifying any interference concerns.

ACKNOWLEDGMENT

This article was presented in part at the IEEE MTT-S International Microwave Symposium (IMS2018), Philadelphia, PA, USA, June 10–15, 2018.

REFERENCES

[1] B. J. Vaughn, D. Peroulis, and A. Fisher, "Mid-range wireless power transfer based on Goubau lines," in *IEEE/MTT-S Int. Microw. Symp. Dig.*, Philedelphia, PA, USA, Jun. 2018, pp. 968–971.
[2] A. Kurs, A. Karalis, R. Moffatt, J. D. Joannopoulos, P. Fisher, and M. Soljačić, "Wireless power transfer via strongly coupled magnetic resonances," *Science*, vol. 317, no. 5834, pp. 83–86, 2007.
[3] M. Xia and S. Aissa, "On the efficiency of far-field wireless power transfer," *IEEE Trans. Signal Process.*, vol. 63, no. 11, pp. 2835–2847, Jun. 2015.
[4] N. Tesla, "Apparatus for transmitting electrical energy," U.S. Patent 1 119 732 A, Dec. 1, 1914.
[5] Z. Dai, Z. Fang, H. Huang, Y. He, and J. Wang, "Selective omnidirectional magnetic resonant coupling wireless power transfer with multiple-receiver system," *IEEE Access*, vol. 6, pp. 19287–19294, 2018.
[6] D. Liu and S. Georgakopoulos, "Cylindrical misalignment insensitive wireless power transfer systems," *IEEE Trans. Power Electron.*, vol. 33, no. 11, pp. 9331–9343, Nov. 2018. Accessed: Aug. 12, 2018. [Online]. Available: IEEE Xplore, ieeexplore.ieee.org
[7] T.-H. Kim, G.-H. Yun, W. Y. Lee, and J.-G. Yook, "Asymmetric coil structures for highly efficient wireless power transfer systems," *IEEE Trans. Microw. Theory Techn.*, vol. 66, no. 7, pp. 3443–3451, Jul. 2018.
[8] B. H. Choi, V. X. Thai, E. S. Lee, J. H. Kim, and C. T. Rim, "Dipole-coil-based wide-range inductive power transfer systems for wireless sensors," *IEEE Trans. Ind. Electron.*, vol. 63, no. 5, pp. 3158–3167, May 2016. Accessed: Aug. 12, 2018. [Online]. Available: IEEE Xplore, ieeexplore.ieee.org
[9] A. Sommerfield, "Ueber die fortpflanzung elektrodynamischer wellen längs eines drahtes," *Ann. Phys.*, vol. 303, no. 2, pp. 233–290, 1899.
[10] G. Goubau, "Surface waves and their application to transmission lines," *J. Appl. Phys.*, vol. 21, no. 11, pp. 1119–1128, 1950.
[11] T. Jeon, J. Zhang, and D. Grischkowsky, "THz Sommerfeld wave propagation on a single metal wire," *Appl. Phys. Lett.*, vol. 86, no. 16, Apr. 2005, Art. no. 161904. Accessed: Dec. 3, 2017. [Online]. Available: https://utol.okstate.edu/sites/default/files/publications/pubs/98_paper96.pdf
[12] J. S. Besnoff and M. S. Reynolds, "Single-wire RF transmission lines for implanted devices," in *Proc. IEEE Biomed. Circuits Syst. Conf. (BioCAS)*, Rotterdam, The Netherlands, Oct. 2013, pp. 222–225. Accessed: Dec. 3, 2017. [Online]. Available: IEEE Xplore, ieeexplore.ieee.org
[13] F. Stulle and J. Bergoz, "The goubau line—Surface waves for bench testing of beam instrumentation at high frequencies," in *Proc. BIW*, Newport News, VA, USA, Apr. 2012, pp. 146–148.
[14] S. R. Best and B. C. Kaanta, "A tutorial on the receiving and scattering properties of antennas," *IEEE Antennas Propag. Mag.*, vol. 51, no. 5, pp. 26–37, Oct. 2009.
[15] D. A. Frickey, "Conversions between S, Z, Y, H, ABCD, and T parameters which are valid for complex source and load impedances," *Trans. Microw. Theory Techn.*, vol. 42, no. 2, pp. 205–211, Feb. 1994. Accessed: Aug. 24, 2018. [Online]. Available: IEEE Xplore, ieeexplore.ieee.org
[16] A. Fisher and D. Peroulis, "Efficient rectifier for wireless power transfer in VHF band," in *Proc. IEEE 19th Wireless Microw. Technol. Conf. (WAMICON)*, Sand Key, FL, USA, Apr. 2018, pp. 1–4.
[17] SAR Measurement Requirements for 100 MHz to 6 GHz. (Aug. 2015). *Federal Communications Commission Office of Engineering and Technology Laboratory Division*. 865664 D01 v01r04. Accessed: Jan. 29, 2019. [Online]. Available: https://apps.fcc.gov/kdb/GetAttachment.html?id=RUMcMDL7fmDLsdRSsbCNoA%3D%3D&desc=865664%20D01%20SAR%20Measurement%20100%20MHz%20to%206%20GHz%20v01r04&tracking_number=28242
[18] FCC Online Table of Frequency Allocations. (Oct. 2018). *Federal Communications Commission Office of Engineering and Technology Policy and Rules Division*. 47 C.F.R. §2.106. Accessed: Jan. 30, 2019. [Online]. Available: https://transition.fcc.gov/oet/spectrum/table/fcctable.pdf

BRIAN J. VAUGHN (S'17) received the B.S. degree in electrical engineering from the University of Illinois, in 2014, and the M.S. degree in electrical engineering from Purdue University, in 2016, where he is currently pursuing the Ph.D. degree with a focus on the use of open-wire transmission lines for wireless power transfer applications.

From 2014 to 2019, he was a Research Assistant with the ARES Group, Purdue University. His research interests include applied and computational electromagnetics, numerical antenna synthesis, and optimization algorithms.

ALDEN FISHER received the B.Sc. degree in electrical engineering from Purdue University. He is currently pursuing the Ph.D. degree with the ARES Lab, under the supervision of Prof. Peroulis. His current research interests include the optical properties of semiconductor devices and their role in reconfigurable, high-frequency electronics. He has explored wireless energy transfer. He is also a member of Eta Kappa Nu. He was the Local MTT Chapter Chair.

DIMITRIOS PEROULIS (S'99–M'04–SM'15–F'17) received the Ph.D. degree in electrical engineering from the University of Michigan at Ann Arbor, Ann Arbor, MI, USA, in 2003.

He is currently the Michael and Katherine Birck Head and the Reilly Professor with the School of Electrical and Computer Engineering, Purdue University, West Lafayette, IN, USA. He has coauthored over 380 journal and conference papers. His current research interests include the areas of reconfigurable electronics, cold-plasma RF electronics, and wireless sensors. He has been a key contributor in developing high-quality widely tunable filters and novel filter architectures based on the miniaturized high-Q cavity-based resonators in the 1–100-GHz range. He is also leading unique research efforts in high-power multifunctional RF electronics based on the cold-plasma technologies.

Dr. Peroulis was a recipient of the National Science Foundation CAREER Award, in 2008. In 2019, he was a recipient of the Tatsuo Itoh Award and, in 2014, he was a recipient of the Outstanding Young Engineer Award, both from the IEEE Microwave Theory and Techniques Society (MTT-S). In 2012, he was a recipient of the Outstanding Paper Award from the IEEE Ultrasonics, Ferroelectrics, and Frequency Control Society (Ferro Electrics Section). His students have been the recipients of numerous student paper awards and other student research-based scholarships. He has been a Purdue University Faculty Scholar and has also received ten teaching awards, including the 2010 HKN C. Holmes MacDonald Outstanding Teaching Award and the 2010 Charles B. Murphy award, which is Purdue University's highest undergraduate teaching honor.